



Luminescent iridium(III)-pyridyl based complexes: tumor inhibitory studies in 4T1 mammary carcinoma mice model

Natesan Sundarmurthy Karthikeyan¹, Shishu Kant Suman^{2*}, Prasad P. Phadnis^{3,4*}, Lalrinawma Zote^{3,5}, Chandan Kumar^{2,6}, Vasanthakumaran Sudarsan^{3,4}

¹Department of Chemistry, Easwari Engineering College, Chennai 600089, Tamil Nadu, India

²Radiopharmaceuticals Division, Bhabha Atomic Research Centre, Mumbai 400085, Maharashtra, India

³Chemistry Division, Bhabha Atomic Research Centre, Mumbai 400085, Maharashtra, India

⁴Chemical Sciences, Homi Bhabha National Institute, Mumbai 400094, Maharashtra, India

⁵Department of Chemistry, Mizoram University, Aizawl 796004, Mizoram, India

⁶Life Sciences, Homi Bhabha National Institute, Mumbai 400094, Maharashtra, India

***Correspondence:** Prasad P. Phadnis, Chemistry Division, Bhabha Atomic Research Centre, Trombay, Mumbai 400085, Maharashtra, India. phadnisp@barc.gov.in; Shishu Kant Suman, Radiopharmaceuticals Division, Bhabha Atomic Research Centre, Trombay, Mumbai 400085, Maharashtra, India. shishu@barc.gov.in

Academic Editor: Renyou Gan, The Hong Kong Polytechnic University, China

Received: November 2, 2025 **Accepted:** April 7, 2026 **Published:** April 28, 2026

Cite this article: Karthikeyan NS, Suman SK, Phadnis PP, Zote L, Kumar C, Sudarsan V. Luminescent iridium(III)-pyridyl based complexes: tumor inhibitory studies in 4T1 mammary carcinoma mice model. *Explor Drug Sci.* 2026;4:1008158. <https://doi.org/10.37349/eds.2026.1008158>

Abstract

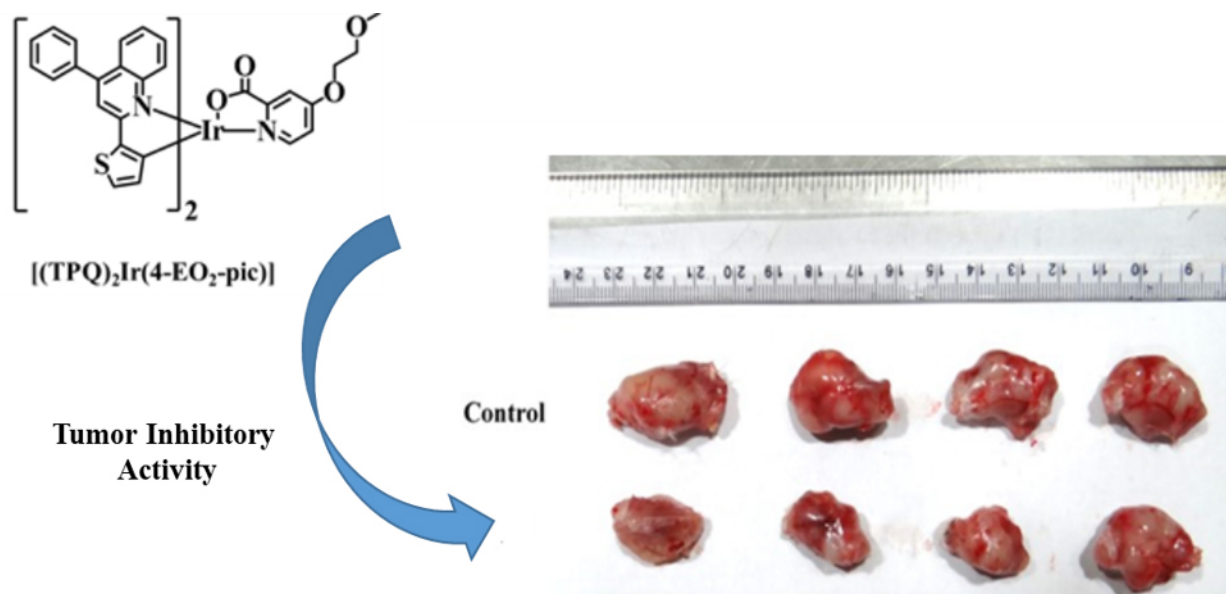
Aim: The iridium(III) [Ir(III)] complexes exhibit anticancer properties, and along with their photoluminescence properties, they can be employed as diagnostic agents. Hence, we have tried to evaluate both properties. For this, the complexes of Ir(III) with pyridyl-based heterocyclic ligands, viz., [(TPQ)₃Ir] (1), [(TPQ)₂Ir(4-EO₂-pic)] (2), and [(ppy)₂Ir(dfmpy)] (3) were prepared and evaluated for their cytotoxicity and emissive properties.

Methods: These complexes were authenticated by NMR (¹H and ¹³C{¹H}) spectroscopy and high-resolution mass spectrometry (HRMS). Their photophysical properties were evaluated by UV-Vis spectroscopy and photoluminescence studies. Among them, [(TPQ)₃Ir] (1) and [(TPQ)₂Ir(4-EO₂-pic)] (2) complexes have exhibited red emission centred at ~600–625 nm range, which is appropriate for bio-imaging. The cellular internalization of [(TPQ)₂Ir(4-EO₂-pic)] (2) complex was investigated by confocal microscopy and flow cytometry at time intervals of 3 h and 6 h after its treatment with cancer cells. These Ir(III) complexes (1–3) were evaluated for their cytotoxicity against 4T1 mammary carcinoma cells by MTT assay. The moderately potent [(TPQ)₂Ir(4-EO₂-pic)] (2) complex was evaluated in vivo against 4T1 mammary carcinoma induced in BALB/c mice.

Results: Among these Ir(III) complexes (1–3), the [(TPQ)₂Ir(4-EO₂-pic)] (2) complex has exhibited moderate cytotoxicity (IC₅₀ ~60 μM) as observed from their evaluations against triple-negative breast cancer (TNBC), a 4T1 mammary carcinoma cell line in vitro by MTT assay. Hence, its in vivo anticancer potency was evaluated by its treatment against 4T1 mammary carcinoma induced in BALB/c mice. This study exhibited tumor-inhibitory activity.



Conclusions: The $[(TPQ)_2Ir(4-EO_2-pic)]$ (2) complex has exhibited a moderate tumor inhibitory property. The presented results have given us insights for designing and developing better Ir(III) complexes in our future endeavours.



Graphical abstract. The red emissive (λ_{em} ~600–625 nm) iridium(III) complex, appropriate for bio-imaging, exhibited cellular internalization, moderate cytotoxicity (IC_{50} ~60 μM) against triple-negative breast cancer 4T1 mammary carcinoma cell lines in vitro as well as in vivo anticancer potency when treated against 4T1 mammary carcinoma induced in BALB/c mice.

Keywords

luminescence, iridium, red emission, 4T1 mammary carcinoma, mice, TNBC

Introduction

Cancer is a life-threatening disease for mankind, which caused ~10 million deaths worldwide in 2022 (WHO Report). For its treatment, chemotherapy is a well-established and convenient approach that employs cisplatin (since 1978) and other platinum(II) [Pt(II)]-based clinical drugs. However, due to physicochemical limitations and severe side effects of Pt(II) drugs, new metal-based drugs were rationally designed and evaluated. Eventually, complexes based on Cu, Zn, Au, Ag, Os, Rh, Ru, and Ir were screened for anticancer activities [1]. Additionally, these elements were useful for imaging, bio-probes, stimuli-responsive drugs, and photosensitizers. Among them, iridium(III) [Ir(III)] based agents have emerged with great potential in the therapeutics of diverse malignancies due to multifunctional, multimodal theragnostic, tumor targeting, and luminescence properties. Recently, some of Ir(III) cyclometalated complexes were reported to exhibit activities like modulators in protein-protein interactions [2], cellular membrane disruption [3], targeting to mitochondria [4], DNA-binding [5], and receptor-targeting [6], and drug interactions with bio-system during treatments. The diverse mechanisms of Ir(III) complexes as anticancer agents are reported. Generally, Ir(III) complexes exhibit anticancer effects via diverse paths, mainly through the generation of ROS (reactive oxygen species), disrupting the functions of mitochondria [7], intercalation with DNA and its damage [8], interfering with cell cycles (usually via G0/G1 arrest) [9], and triggering apoptosis via caspase activation [10]. These complexes usually target lysosomes [11], increasing ROS [12] and Ca signalling pathways [13], leading to cell death via various mechanisms like autophagy or ferroptosis [14]. They have exhibited the ROS production to kill cancerous cells via the PDT modality also. Additionally, the reports have revealed that Ir(III) complexes exhibit a novel mechanism of anticancer action that is different from Pt(II) based drugs. Along with therapeutic properties, the luminescent Ir(III) complexes have exhibited their utility for diagnostic applications owing to their high cellular permeability, long living red to

near-infrared (NIR) emissions in the biological window useful for bio-imaging [15]. Additionally, Ir(III) complexes have exhibited utility as probes for effective detection of hypoxic tissues [16]. Recently, the Ir(III) complexes have exhibited oxygen and Hg²⁺ species sensing [17] as well as detection of SO₂ derivatives in mitochondria of living cells [18].

At this point, it's worth discussing the triple-negative breast cancer (TNBC) and the representative strategies or drugs for its treatment. It is highly aggressive, difficult to treat, and characterized by a high recurrence rate, leading to metastasis and death. However, if detected in the early stage, control of breast cancer is possible. Usually, chemotherapy is performed prior to radiotherapy. But the impressive anti-tumor activity can be achieved by radiotherapy in combination with surgery, chemotherapy, and endocrine therapy (or hormone therapy) as well as immunotherapy, but still, the radiotherapy leads to complications, although the breast radiotherapy [19] also reduces the probability of cancer recurrence, but it's a crucial part of treatment. Other novel therapies have also been employed for treating the TNBC [20]. Additionally, Mulligan et al. [21] have revealed the complete cure of breast cancer by the ErSO-TFPy [3-(4-hydroxyphenyl)indoline-2-one-tetrafluoropyrrolidine] anticancer compound, but it has not reached clinical practice. The development of TNBC treatment agents is essential. Hence, efforts for new drugs with small organic or organometallic compounds or repurposing of known drugs are going on. At this point, it is worth discussing representative organic drugs also. Tamoxifen, a Food and Drug Administration (FDA)-approved (1998) organic drug, is used to treat breast cancer. It is a drug which cure estrogen receptor (ER) α -positive breast cancer or other gene interactions [22] and some ER-negative breast cancers also [23]. In the case of TNBC, the absence of effective therapeutic targets and its aggressive nature create difficulties for its curation. It has been found that administration of only tamoxifen has exhibited its potency as an anti-proliferative agent with reasonable certainty [24], or may not be very effective. But its administration, along with adjuvant drugs and drug delivery systems (DDS), has enhanced its efficacy to treat TNBC. However, in the present time, surgery is still recommended for better results. From this discussion, it is inferred that early detection is essential to control TNBC, while in advanced stages of TNBC, a complete cure is less probable, but management of a chronic condition can be achieved by using novel therapies. The important factors for curing TNBC depend mainly on the stage of cancer progression and its response to treatment. Hence, the search for new and effective drugs is still going. Along with this, external beam radiation technique and the internal beam therapy, i.e., brachytherapy, are known for TNBC treatment. Additionally, it is found that alone radiotherapy is not effective to cure breast cancer, but it may be used to treat breast cancer at almost every stage. Hence, radiotherapy is usually used in combination with conventional therapies. The women undergone radiotherapy may experience side effects like skin irritation, fatigue, and swelling. Till today, no Ir(III) complex has been approved by the FDA for cancer treatment, but a γ -emitter iridium-192 (¹⁹²Ir) has been used for brachytherapy for treating cancers by radiotherapy [25]. Furthermore, the Xofigo[®] (Xofigo[®] eBx system) was approved by the FDA, USA, for the treatment of early breast cancer (EBC) in 2006 [26]. Additionally, the naturally occurring drugs have also exhibited potency to treat breast cancers. The diverse compounds isolated from natural fruits have exhibited their utility for diverse cancer treatments. Recently, Kalhori et al. [27] have reported the remarkable potential of cellulose nanocrystals (CNCs) isolated from *Citrus medica* L. pericarp, which was found to be biocompatible and exhibited interaction between HMG-CoA reductase (HMGR) and reduced catalytic activity and changes in the secondary structure of HMGR. Hence, HMGR inhibitors are known for their use in the treatment of cases of breast cancer [28]. Additionally, Kaffash et al. [29] have evaluated the protein-protein interactions by spectroscopic and molecular simulations to understand the biomedical activities of kaempferol (KMP), which is a natural flavonoid known to exhibit diverse biomedical properties, especially anticancer properties. The studies based on docking and molecular dynamics simulations have revealed the mechanism of KMP binding with human serum albumin (HAS) and human holo-transferrin (HTF).

In view of this, to fulfil our research interest of design and evaluation of metallodrugs for TNBC treatment, we have synthesized known Ir(III) complexes with pharmacologically active pyridyl-based moieties having clinical relevance. In this study, some of Ir(III) complexes have exhibited emissions in the

tissue transparency window but poor cytotoxicity, offering their possible use in bio-imaging. Additionally, one of the Ir(III) test complexes exhibited cellular internalization and emission in the tissue transparency window, along with moderate cytotoxicity against TNBC cell lines in vitro, as well as tumor inhibitory activities against highly aggressive 4T1 mammary carcinoma induced in BALB/c mice (xenograft model). This complex has the scope for further investigations and may find its utility for theragnostic applications in TNBC management. Our preliminary results are reported herein.

Materials and methods

All chemicals and reagents used during synthesis and cell culture experiments were purchased from commercial chemical manufacturers, viz., Sigma-Aldrich and TCI (Tokyo Chemical Industry). These chemicals were used without further purification. All the reactions were performed under an inert atmosphere of nitrogen (N₂) flow. Doubly distilled water was used throughout the syntheses and all the biological experiments. The nuclear magnetic resonance (NMR) spectra were recorded in CDCl₃ (deuterated chloroform) as a solvent on a Bruker 400 MHz NMR spectrometer, and the chemical shifts (δ) are expressed in ppm (parts per million). The resonances in NMR spectra were relative to δ 7.27 ppm (for ¹H) and δ 77.16 ppm (for ¹³C{¹H}) as internal standards owing to 0.5% CHCl₃ in CDCl₃ solvent. The mass analyses by HRMS (high-resolution mass spectrometry) were performed using a JEOL GC Mate II Mass spectrometer. The absorption spectra were measured using a Jasco V-750 spectrophotometer. The luminescence measurements were performed on a Jasco FP-8300 instrument. The MDA-MB-231 and 4T1 cancer cell lines used for in vitro or in vivo cytotoxicity studies were purchased from the American Type Culture Collection (ATCC). The cytotoxicity evaluation of the Ir(III) complexes against cancer cells was performed by 3-[4,5-dimethylthiazol-2-yl]-2,5-diphenyl tetrazolium bromide (MTT) assay. The cellular internalization of selected Ir(III) complexes was studied by imaging via confocal microscopy. The microscope IX3SVR utilizes an Olympus IX83 inverted microscope, in which the laser beams are incident over a back focal plane of a 40 × 0.75 numerical aperture (NA) apochromatic objective lens of Olympus. The illuminance at the samples was regulated by using FLUOVIEW software. An array of Z-planes was collected at every 400 nm by employing a motor-equipped platform, followed by the Z-stacking in order to produce 3D (three-dimensional) images. The cellular images by fluorescence mode were recorded using 470/590 nm ($\lambda_{\text{ex}}/\lambda_{\text{em}}$) and 402/460 nm ($\lambda_{\text{ex}}/\lambda_{\text{em}}$) wavelengths for test Ir(III) complexes and 4',6-diamidino-2-phenylindole (DAPI), respectively. The Olympus CellSens software, along with Adobe Photoshop (7.0), was used in order to process the images. Additionally, the internalization was evaluated by flow cytometry on the Guava® easyCyte™ flow cytometer. The data obtained from flow cytometry was analyzed via employing a Guava® InCyte™ software obtained from the Luminex Corporation, Austin, Texas, USA. The tumor inhibitory activities were evaluated against a 4T1 mammary carcinoma induced in BALB/c mice, which were provided by the Animal House Facility of BARC, Mumbai (Approval no.: BAEC No. 19/22; dated 06/12/2023).

Synthesis

Synthesis of [(TPQ)₃Ir] (1) [30]

A mixture of IrCl₃·H₂O (0.055 g, 0.174 mmol), 4-phenyl-2-(thiophen-2-yl) quinoline (TPQ) (1 g, 1.74 mmol) (for synthesis procedure scheme, [Figure S1](#)), and silver trifluoroacetate (0.15 g, 0.696 mmol) were dissolved in 10 mL glycerol at room temperature (RT) followed by refluxing the resulted reaction mixture at 180°C for 24 h. As the reaction was completed, distilled water (100 mL) was added in reaction mixture and extracted for 3 times by 30 mL of dichloromethane (CH₂Cl₂) (3 × 30 mL) followed by further washing with a brine solution (aqueous NaCl) and an organic phase of CH₂Cl₂ was dried by suspending an anhydrous NaSO₄ (~2 g for 30 min) to remove traces of water. The CH₂Cl₂ phase was dried in vacuo, and the obtained crude product was purified by chromatographic technique by using ethyl acetate (CH₃COOCH₂CH₃) and hexane (C₆H₁₄) mixture (in 1:4 v/v ratio) as eluent, which afforded a red powder of [(TPQ)₃Ir] (1) complex (0.125 g, 66%) on drying the eluted phase ([Figure S1](#)). The purified [(TPQ)₃Ir] (1) complex was characterized by NMR spectroscopy and HRMS analysis. ¹H NMR (400 MHz, CDCl₃): δ 8.06–8.04 (d, 3H), 7.73–7.71 (d, 3H), 7.62–7.49 (m, 18H), 7.16–7.10 (m, 6H), 6.78–6.74 (t, 3H), 6.10–6.09 (d, 3H); ¹³C{¹H} NMR

(CDCl₃): δ 161.79, 158.71, 149.63, 149.34, 138.13, 138.88, 134.68, 129.73, 129.54, 128.56, 128.50, 127.39, 126.23, 124.91, 124.38, 118.44 ppm. HRMS [M + H]⁺: m/z found 1,050.1757, calcd. for [(TPQ)₃Ir] (1) complex 1,051.3330.

Synthesis of [(TPQ)₂Ir(4-EO₂-pic)] (2) [17]

The titled complex was synthesized in two steps, as shown in [Figure S6](#).

Step 1: Synthesis process of μ-chloro-bridged dimer [(TPQ)₂Ir(μ-Cl)₂Ir(TPQ)₂]

The mixture of compounds, TPQ (1.25 g, 4.35 mmol) and IrCl₃·H₂O in 20 mL of water and 2-ethoxy ethanol (in a 3:1 v/v ratio) was refluxed at 140°C for 24 h in an inert atmosphere of N₂ gas until a red precipitate appeared. This red precipitate was filtered out and washed with doubly distilled water and then dried in vacuo at 120°C, yielding [(TPQ)₂Ir(μ-Cl)₂Ir(TPQ)₂] in fair yields (0.84 g, 60%).

Step 2: Synthesis of [(TPQ)₂Ir(4-EO₂-pic)]

The titled Ir(III) complex [(TPQ)₂Ir(4-EO₂-pic)] was prepared by treatment of the bridged complex (from step 1) with 4-chloropicolinic acid. Accordingly, a mixture of 4-chloropicolinic acid (0.66 g, 3.82 mmol), μ-chloro-bridged dimer (1 g, 0.765 mmol), and sodium carbonate (0.8 g, 7.65 mmol) was prepared in 20 mL of 2-ethoxy ethanol. Then the resulting mixture was refluxed under an inert atmosphere of N₂ gas for 12 h. The advancement in reaction was tracked by TLC (thin-layer chromatography). After the reactants had reacted completely, resulted reaction mixture was allowed to cool to ambient temperature. To this, distilled water (100 mL) was added, and the solution was extracted by using CH₃COOCH₂CH₃, and this organic phase was dried over anhydrous NaSO₄ (~5 g for ~30 min). After drying the organic phase in vacuo, the obtained crude product was purified by chromatography using an ethyl acetate and C₆H₁₄ mixture in a 1:4 v/v ratio as an eluent, which afforded a purified, red colored Ir(III) complex (0.39 g, 58%). The ultraviolet-visible (UV-Vis) absorbance was recorded in acetonitrile ([Figure S10](#)). This complex [(TPQ)₂Ir(4-EO₂-pic)] was analyzed with NMR spectroscopy and HRMS analysis. ¹H NMR (400 MHz, CDCl₃): δ 8.79–8.77 (d, 1H, Ar H), 7.98–7.95 (m, 2H, Ar H), 7.76–7.68 (m, 4H, Ar H), 7.63 (s, 1H, Ar H), 7.59–7.57 (m, 10H, Ar H), 7.42–7.30 (m, 3H, Ar H), 7.20–7.12 (q, 3H, Ar H), 6.86 (t, 1H, Ar H), 6.67–6.66 (d, 1H, Ar H), 6.20–6.18 (d, 1H, Ar H), 4.18–4.05 (q, 2H; CH₂), 3.78–3.67 (t, 2H; CH₂), 3.57–3.46 (q, 2H; CH₂), 1.22–1.14 (t, 3H; CH₃); ¹³C{¹H} NMR (400 MHz, CDCl₃): δ 172.53, 166.72, 165.35, 153.67, 153.59, 153.04, 151.39, 151.35, 149.93, 149.02, 147.03, 141.58, 139.31, 137.95, 137.48, 137.44, 134.84, 133.61, 132.09, 130.90, 130.03, 129.88, 129.21, 129.08, 128.95, 127.97, 127.70, 127.55, 126.48, 126.38, 125.76, 125.64, 124.85, 124.64, 124.14, 117.97, 116.99, 111.91, 15.04 ppm. HRMS: m/z found 975.1774 [M⁺], calcd. for [(TPQ)₂Ir(4-EO₂-pic)] (2): 975.1700.

Synthesis of (ppy)₂Ir(dfppy) (3) [31]

The titled complex was synthesized in two steps, as shown in [Figure S11](#).

Step 1: Synthesis of μ-chloride bridged dimer [(ppy)₂Ir(μ-Cl)₂Ir(ppy)₂]

The phenylpyridine (1.5 g, 9.65 mmol) and IrCl₃·H₂O (1.15 g, 3.86 mmol) were dissolved in 20 mL of 3:1 v/v distilled water and 2-ethoxy ethanol. Then the resulting reaction mixture was refluxed at 140°C for 20 h under an inert atmosphere of N₂ gas. After cooling to ambient temperature, the yellow colored precipitate was formed, which was filtered out, followed by washing with methanol (CH₃OH) and a mixture of distilled water and methanol (in a 1:3 v/v ratio) and solvent was evaporated in vacuo to obtain a titled compound, [(ppy)₂Ir(μ-Cl)₂Ir(ppy)₂] (1.34 g, 52%).

Step 2: Synthesis of [(ppy)₂Ir(dfppy)]

The [(ppy)₂Ir(μ-Cl)₂Ir(ppy)₂] (1 g, 0.765 mmol), triethylamine (0.205 g, 2.04 mmol), dfppy (0.48 g, 2.33 mmol), and acetylacetone (0.205 g, 2.04 mmol) were dissolved in dried ethylene glycol [(CH₂OH)₂] and refluxed under an inert N₂ atmosphere for 72 h. Later, this reaction mixture was cooled to RT, and then the crushed ice was poured into this reaction mixture. Then this reaction mixture was extracted with CH₂Cl₂ (3 × 150 mL), and this organic phase was dried by suspending with anhydrous NaSO₄ for 30 min. Then the

crude compound was column chromatographed to purify it by using ethyl-acetate and C₆H₁₄ mixture (in 1:3 v/v ratio) as eluent to afford [(ppy)₂Ir(dfpmpy)] (**3**) as a green compound (0.4 g, 60%). The purified Ir(III) complex [(ppy)₂Ir(dfpmpy)] (**3**) was authenticated by NMR spectroscopy and HRMS analysis. ¹H NMR (400 MHz, CDCl₃): δ 8.10–8.07 (d, 2H), 7.90–7.85 (d, 1H), 7.64–7.35 (m, 7H), 6.93–6.66 (m, 7H), 6.36–6.22 (m, 4H), 2.41 (s, 3H) ppm. ESI-MS [M + H]⁺: m/z found 705.16, calcd. for (ppy)₂Ir(dfpmpy) (**3**): 704.80.

Cell culture experiments

The TNBC, viz., MDA-MB-231 and 4T1, were cultivated in DMEM (Dulbecco's modified Eagle medium) medium supplemented with 10% FBS (fetal bovine serum) at 37°C in a humidified 5% CO₂ incubator. These cancer cells were harvested by using 0.025% trypsin in supporting medium (DMEM) containing 10% FBS. The evaluations against cancer cells were performed by the MTT assay.

Cellular internalization study of [(TPQ)₂Ir(4-EO₂-pic)] (**2**) complex in TNBC by using confocal microscopy and flow cytometry

To evaluate cellular uptake of [(TPQ)₂Ir(4-EO₂-pic)] (**2**) complex in TNBC cells, MDA-MB-231 and 4T1 cell lines in vitro, fluorescence confocal microscopy [32, 33] and flow cytometry studies were carried out. In studies by confocal imaging, the TNBC cell lines were grown and harvested. The cancer cells 4T1 and MDA-MB-231 (5 × 10⁴) were seeded over the circular glass coverslips in a 24-well plate and cultured overnight for attachment. Later, the cells (*n* = 3) were incubated with a [(TPQ)₂Ir(4-EO₂-pic)] (**2**) complex of 10 μM concentration for 3 h and 6 h. After incubation (37°C), these cells were washed with PBS (phosphate-buffered saline) for 2 times in order to remove non-internalized drug formulation, and then they were fixed with a fixative agent, 4% para-formaldehyde. The cells were then stained with DAPI. Then we have employed a confocal microscope (IX3SVR) by using the Olympus IX83 inverted microscope along with laser beams focused on the back focal plane of a 40 × 0.75 NA apochromatic objective lens of Olympus. The intensity of incident laser illumination over the samples was modulated by using FLUOVIEW software. The data from Z-planes was obtained at each 400 nm using a motor-driven platform, and then the Z-stacking was performed in order to afford the 3D images. The fluorescence-based images were recorded using 554/625 nm and 356/460 nm wavelengths as λ_{ex}/λ_{em} for complex [(TPQ)₂Ir(4-EO₂-pic)] (**2**) complex and DAPI, respectively. The obtained fluorescence images were then processed by employing the Olympus CellSens software and with the help of Adobe Photoshop (version 7.0) software.

To investigate the cellular uptake evaluation by flow cytometry, the TNBC, 4T1, and MDA-MB-231 cell lines were cultured as mentioned previously, and 1 × 10⁵ cells were allowed to seed in a 12-well plate. After an incubation for 8–10 h (overnight), the seeded cells were then treated with [(TPQ)₂Ir(4-EO₂-pic)] (**2**) complex for 3 h and 6 h. After the incubation, the treated cells were rinsed two times with PBS solution (pH 7.4) in order to get rid of excess pharmacological agent, i.e., [(TPQ)₂Ir(4-EO₂-pic)] (**2**) complex. Then these cells were subjected to harvest followed by acquisition of images by employing Incyte software module in a Guava EasyCyte Flow Cytometer, and then were analyzed by use of Cyflogic software in order to detect a cellular internalization of a test [(TPQ)₂Ir(4-EO₂-pic)] (**2**) complex.

Cytotoxicity evaluations of Ir(III) complexes against cancer cell lines by MTT assay

The 4T1 mammary carcinoma cells were allowed to grow as monolayers in 10% FBS supplemented DMEM medium, added with 100 μg/mL of an antibiotic (streptomycin) and penicillin (100 U/mL) at 37°C under 5% CO₂ as well as humidified air. The prepared stocks of [(TPQ)₃Ir] (**1**), [(TPQ)₂Ir(4-EO₂-pic)] (**2**), and [(ppy)₂Ir(dfpmpy)] (**3**) complexes in dimethyl sulfoxide (DMSO) and/or water were added to the cultured medium to obtain the desired concentrations. The concentration of solvent DMSO in control, Ir(III) complexes (**1–3**) treated cells was maintained constant within the permissible limits (0.05%) of toxicity. To evaluate the cytotoxicity, 7 × 10³ cells in each well in a 96 well-plate were allowed to seed, followed by treatment with concentration (1–100 μM) of Ir(III) **1–3** test complexes for ~48 h, and then evaluated by MTT assay by following standard methods [34]. The cytotoxicity (in %) was calculated by following the decrease in absorbance (at λ_{max} 550 nm) for a purple formazan product formed in this assay after treatment of Ir(III) **1–3** complexes with cancer cell lines, as compared to the control (Equation 1).

$$\% \text{ Viability} = \frac{\text{Mean OD treated}}{\text{Mean OD control}} \times 100 \text{ (Equation 1)}$$

In vivo anticancer studies against the 4T1 mammary carcinoma model in BALB/c mice

The evaluation of anticancer activity of [(TPQ)₂Ir(4-EO₂-pic)] (**2**) complex was performed in vivo in animal models as a part of further studies of the test complex.

Humane endpoint

To minimize the suffering or pain of animals, we have followed the guidelines of India's CPCSEA (Committee for the Purpose of Control and Supervision of Experiments on Animals), which regulates the use of animals in research and experimentation, with the reference no. 106/GO/RBi/S/99/CPCSEA dated 12.08.2022.

The in vivo anticancer activity of [Ir(TPQ)₂(4-EO₂-pic)] (**2**) complex was evaluated by its intra-tumoral administration against 4T1 mammary carcinoma induced in BALB/c mice. In this experiment, for evaluating the in vivo therapeutic effect of [(TPQ)₂Ir(4-EO₂-pic)] (**2**) complex, the 4T1 tumors were induced subcutaneously in BALB/c mice by injecting 4T1 cells (1×10^4). The solution of [(TPQ)₂Ir(4-EO₂-pic)] (**2**) complex in PBS (10 mg/kg) was injected intra-tumorally in 4T1 tumors grafted in BALB/c mice ($n = 6$). The buffer control mice ($n = 6$) were also injected intra-tumorally with PBS buffer. Subsequently, the tumor size was measured by using a Vernier calliper on every alternate day, and overall treatment was monitored till the tumor size reached 1,500 mm³, which took about 17 days. The tumor volume was calculated by the formula (Equation 2) as:

$$\text{Tumor volume} = \frac{\pi}{6} \times (\text{length} \times \text{width} \times \text{height}) \text{ in cm (Equation 2)}$$

Euthanasia

The mice were sacrificed via saturated CO₂ euthanasia, i.e., use of a high concentration of CO₂ in a euthanasia chamber till death of the mice.

Comparison of tumor volumes

From the data of tumor volumes calculated, the relative tumor growth rate was plotted against the number of days post-treatment in response to treatment of [(TPQ)₂Ir(4-EO₂-pic)] (**2**) complex and a control group as well.

Statistical analysis

All the data have been presented in the form of mean \pm SD (standard deviation). It was followed through the analyses of statistical differences among diverse mean data as carried out by a one-way analysis of variance (ANOVA), followed by Tukey's multiple comparison test with the help of software (Graphpad Prism 6). The mean difference between groups was statistically compared by employing an unpaired *t*-test in the same software. The differences with values of $P < 0.05$ (*) or $P < 0.01$ (**) have been considered statistically important.

Results

Synthesis

The Ir(III) complexes (**1–3**) were synthesized by complexation reactions of IrCl₃·H₂O with the corresponding pyridyl-based N-heterocyclic ligands with appropriate substituents or polar organic chains on the pyridyl moiety (Figure 1) [17, 30, 31]. These complexes were authenticated with NMR spectroscopy and HRMS. The ¹H NMR (in CDCl₃) exhibited resonances for aryl protons ranging from 6–9 ppm, and in the case of complexes (**2**) and (**3**), the aliphatic protons exhibited resonances from 1–4 ppm (Figures S2, S7, and S12). The ¹³C{¹H} NMR spectra (in CDCl₃) of aryl heterocyclic groups these complexes exhibited resonances in chemical shift ranging from 120–160 ppm while in case of [(TPQ)₂Ir(4-EO₂-pic)] (**2**) and [(ppy)₂Ir(dfmpy)] (**3**) complexes the aliphatic groups attached to heterocyclic rings exhibited resonances in range of 15–70 ppm (Figures S3 and S8).

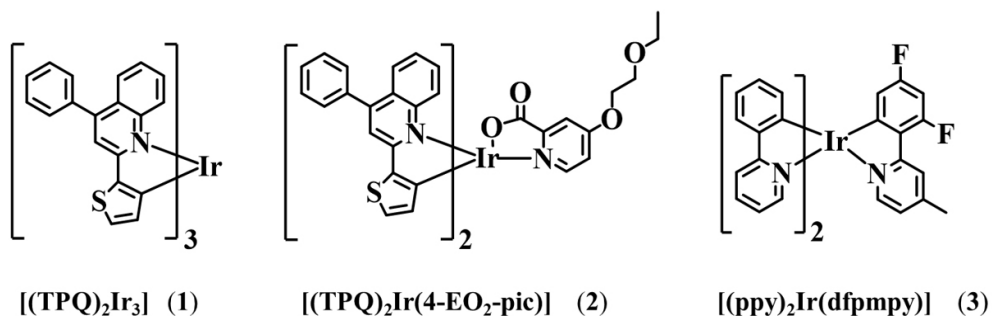


Figure 1. Ir(III) complexes (1–3) with pyridyl-based ligands.

The HRMS analyses were performed, which exhibited the molecular ion peaks corresponding to the exact molecular masses of Ir(III) complexes (1–3) with specific isotopic patterns (Figures S4, S9, and S13).

UV-Vis and photoluminescence studies

The UV-Vis and photoluminescence (PL) features of $[(\text{TPQ})_3\text{Ir}]$ (1) complex were recorded in acetonitrile (Figure S5). It exhibits two absorbance bands centred at wavelengths 312 nm and 421 nm, as well as a clear shoulder at 459 nm. A weak band was also observed at wavelength 578 nm (Figure S5a). The PL spectrum of $[(\text{TPQ})_3\text{Ir}]$ (1) complex is presented in Figure S5b. Upon the excitation at 430 nm, the PL spectra of $[(\text{TPQ})_3\text{Ir}]$ (1) complex exhibit a red emission peak at 601 nm [30]. The UV-Vis absorption and emission (PL) spectra of $[\text{Ir}(\text{TPQ})_2(4\text{-EO}_2\text{-pic})]$ (2) complex were recorded at ambient temperature in acetonitrile. The intense absorptions in the ultraviolet region 280–370 nm were observed. The complex also displayed weak visible bands in the range of 406–576 nm (Figure S8). The PL measurements of $[(\text{TPQ})_2\text{Ir}(4\text{-EO}_2\text{-pic})]$ (2) complex exhibited emission centred at wavelength ~ 625 nm upon excitation by 583, 554, and 443 nm wavelengths (Figure 2) [17].

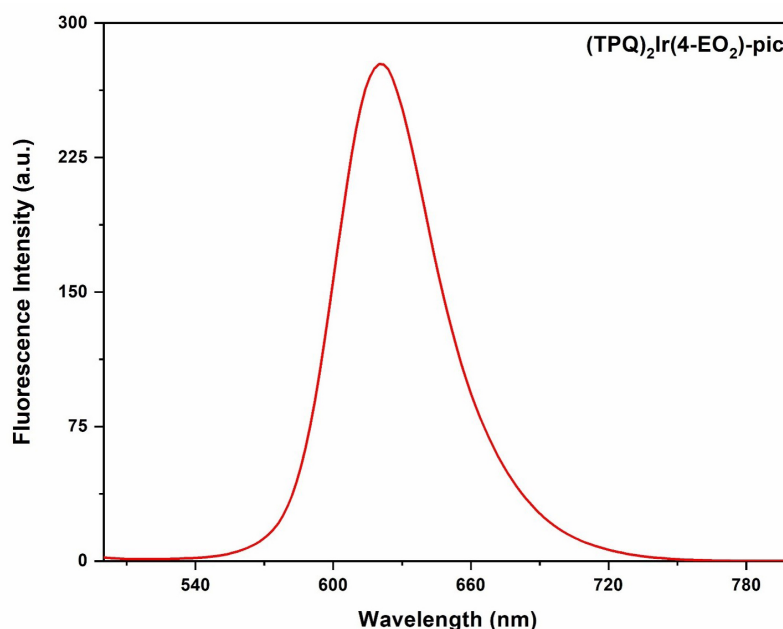


Figure 2. Emission spectrum of $[\text{Ir}(\text{TPQ})_2(4\text{-EO}_2\text{-pic})]$ (2) complex ($\lambda_{\text{ex}} = 554$ nm; $\lambda_{\text{em}} = 625$ nm) (in acetonitrile).

The UV-Vis and PL spectra of $[(\text{ppy})_2\text{Ir}(\text{dfpmPy})]$ (3) complex were recorded in acetonitrile. The intense UV-Vis absorption bands are observed at 292 and 291 nm. Additionally, the band at 354 nm was also observed (Figure S14a). The emission spectra (PL) of $[(\text{ppy})_2\text{Ir}(\text{dfpmPy})]$ (3) complex exhibited an intense PL bluish-green emission band with its maximum at 510 nm upon excitation by 465 nm (Figure S14b) [31].

Cytotoxicity evaluation in-vitro

The test Ir(III) complexes (**1–3**) were evaluated for their cytotoxic potency against TNBC 4T1 mammary carcinoma cell lines by MTT assay and flow cytometric analysis (in vitro).

Cytotoxicity evaluations against cancer cell lines by MTT assay

The treatment of 4T1 mammary cancer cells with Ir(III) complexes (**1–3**) was observed in vitro for 48 h. The $[(\text{TPQ})_2\text{Ir}(4\text{-EO}_2\text{-pic})]$ (**2**) complex was found to be cytotoxic with substantially higher efficiency ($\text{IC}_{50} = 60 \mu\text{M}$) as compared to $[(\text{TPQ})_3\text{Ir}]$ (**1**) and $[(\text{ppy})_2\text{Ir}(\text{dfpmpy})]$ (**3**) complexes, which have been depicted in Figure 3.

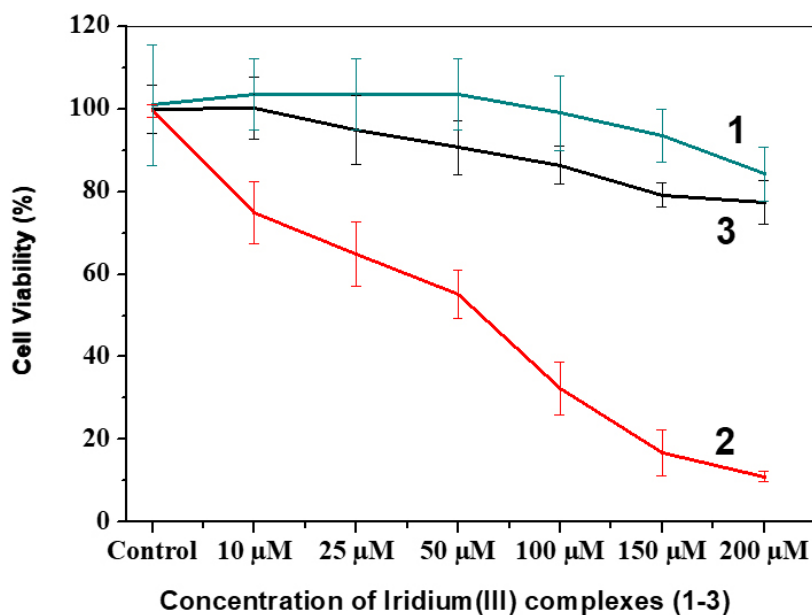


Figure 3. Cytotoxicity evaluations of Ir(III) complexes against 4T1 mammary cancer cells.

Cellular internalization studies of $[(\text{TPQ})_2\text{Ir}(4\text{-EO}_2\text{-pic})]$ (**2**) complex in TNBC cancer cell lines by flow cytometry

The test $[\text{Ir}(\text{TPQ})_2(4\text{-EO}_2\text{-pic})]$ (**2**) complex was evaluated for its cellular internalization in MDA-MB-231 and 4T1 mammary carcinoma cell lines by flow cytometry at time intervals of 3 h and 6 h after treatment (Figure 4). The flow cytometry studies for cellular uptake evaluation of $[\text{Ir}(\text{TPQ})_2(4\text{-EO}_2\text{-pic})]$ (**2**) complex exhibited enhancement in uptake with an increase in incubation time in both TNBC cells, i.e., MDA-MB-231 and 4T1 mammary carcinoma cells. Comparatively, cellular uptake of $[\text{Ir}(\text{TPQ})_2(4\text{-EO}_2\text{-pic})]$ (**2**) complex in MDA-MB-231 cells was high ($P < 0.05$) with $17.89 \pm 1.31 \times$ geomean as compared to $14.01 \pm 0.29 \times$ geomean in 4T1 cells at 6 h after treatment (Figure 4). Additionally, the flow cytometry overlay histogram (at 6 h) exhibiting both unstained and $[\text{Ir}(\text{TPQ})_2(4\text{-EO}_2\text{-pic})]$ (**2**) treated 4T1 and MDA-MB-231 cells for comparison has been presented in Figure S15. Furthermore, the results analysis bar chart correlating with cellular internalization of $[\text{Ir}(\text{TPQ})_2(4\text{-EO}_2\text{-pic})]$ (**2**) in both the cells has been presented as Figure S16.

Cellular internalization studies by confocal microscopy

The cellular internalization of $[\text{Ir}(\text{TPQ})_2(4\text{-EO}_2\text{-pic})]$ (**2**) complex was also evaluated by cellular imaging using the red emissive property of this test complex. The MDA-MB-231 and 4T1 mammary carcinoma cell lines were treated with the $[(\text{TPQ})_2\text{Ir}(4\text{-EO}_2\text{-pic})]$ (**2**) complex and its real time internalization was monitored by confocal microscopy at 3 h and 6 h which revealed that, the cellular uptake increased with time and at the end of 6 h the complex $[(\text{TPQ})_2\text{Ir}(4\text{-EO}_2\text{-pic})]$ (**2**) complex has much higher internalization in TNBC MDA-MB-231 cancer cells as compared to 4T1 mammary carcinoma cells (Figure 5) which is in good agreement with flow cytometry results as discussed earlier.

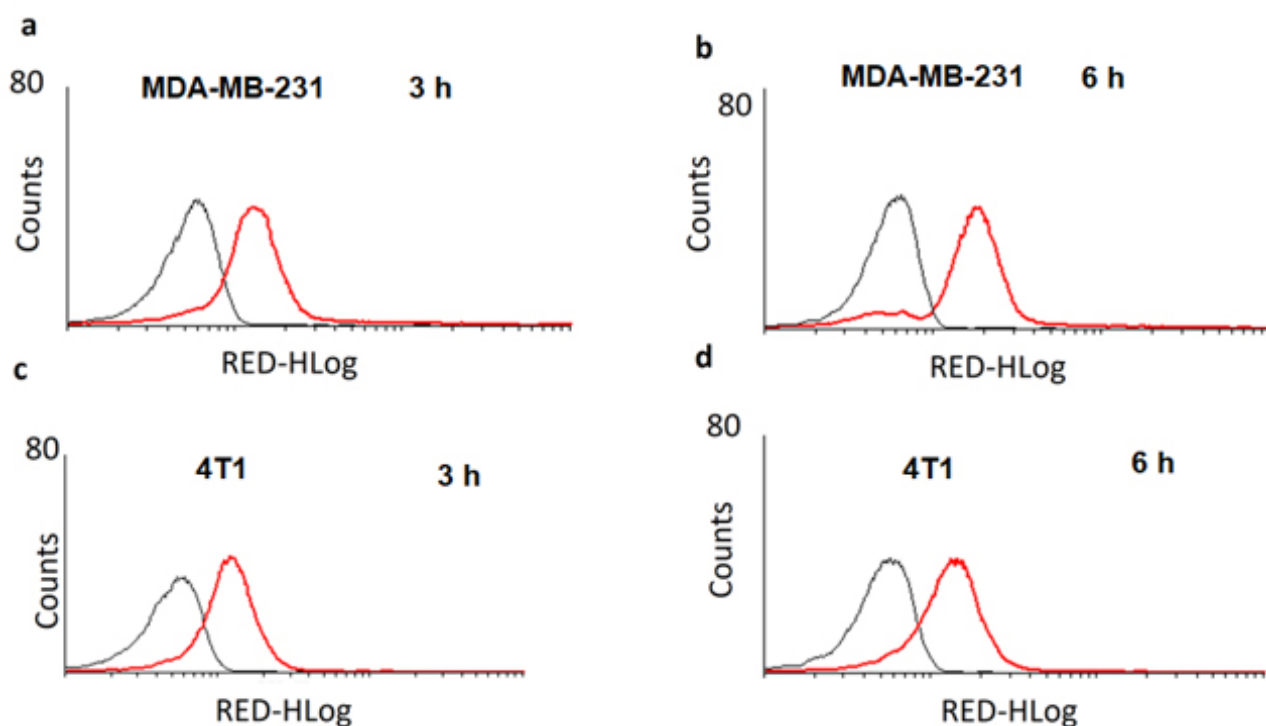


Figure 4. Cellular internalization of $[\text{Ir}(\text{TPQ})_2(4\text{-EO}_2\text{-pic})]$ (**2**) complex by flow cytometry in triple-negative breast cancer cells MDA-MB-231 at 3 h (a), MDA-MB-231 at 6 h (b), 4T1 at 3 h (c), and 4T1 at 6 h (d) (Counts is no. of cells & RED-HLog is the fluorescence emitted by the compound internalized in the cells).

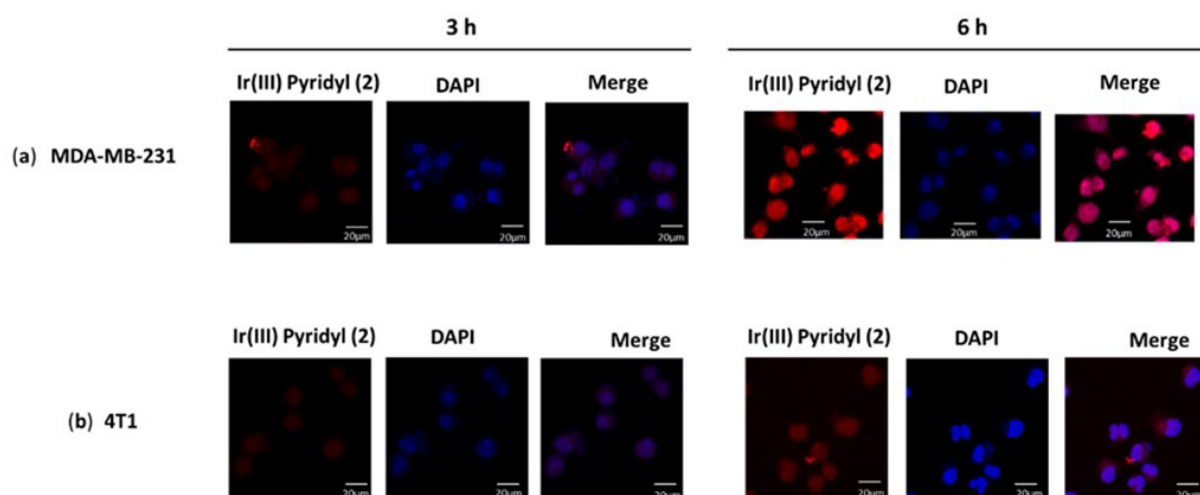


Figure 5. Evaluation of cellular internalization of $[\text{Ir}(\text{TPQ})_2(4\text{-EO}_2\text{-pic})]$ (**2**) complex in MDA-MB-231 (a) and in 4T1 cells (b) by confocal microscopy at 3 and 6 h.

These studies revealed that the test $[\text{Ir}(\text{TPQ})_2(4\text{-EO}_2\text{-pic})]$ (**2**) complex exhibits cellular internalization and accumulation in the nucleus (Figures 4 and 5).

Antitumor activities evaluation in vivo in BALB/c mice models

After evaluating the test Ir(III) complexes (**1-3**) in vitro against both the TNBC cell lines and observing the moderate cytotoxicity of $[\text{Ir}(\text{TPQ})_2(4\text{-EO}_2\text{-pic})]$ (**2**) complex, we planned to evaluate $[\text{Ir}(\text{TPQ})_2(4\text{-EO}_2\text{-pic})]$ (**2**) complex against the tumor models induced in BALB/c mice in order to enhance our studies.

Tumor growth inhibition studies by treatment of $[\text{Ir}(\text{TPQ})_2(4\text{-EO}_2\text{-pic})]$ (**2**) complex

We observed intermittently for 17 days that the test $[\text{Ir}(\text{TPQ})_2(4\text{-EO}_2\text{-pic})]$ (**2**) complex has inhibited the growth of tumors as observed from the plot of measured tumor volume against the number of days of treatment progress (Figure 6). On the 17th day, the experimental mice were sacrificed, and the extracted

tumors from control and $[(\text{TPQ})_2\text{Ir}(4\text{-EO}_2\text{-pic})]$ (**2**) complex-treated mice were compared (Figure 7), which revealed the tumor inhibitory potency of $[\text{Ir}(\text{TPQ})_2(4\text{-EO}_2\text{-pic})]$ (**2**) complex. In this study, the tumor volume difference at the end of treatment was control: $1,322 \pm 56 \text{ mm}^3$ vs. treatment $1,031.3 \pm 78.4 \text{ mm}^3$, which is statistically different, $P < 0.0001$.

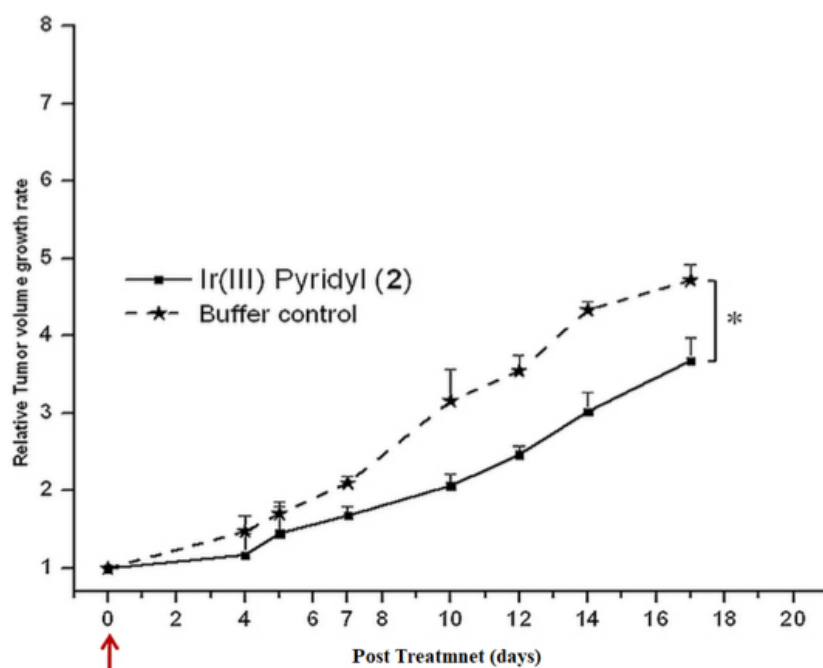


Figure 6. Tumor regression in BALB/c mice after treatment with $[\text{Ir}(\text{TPQ})_2(4\text{-EO}_2\text{-pic})]$ (**2**) complex. The data has been analysed by using a two-tailed unpaired *t*-test.

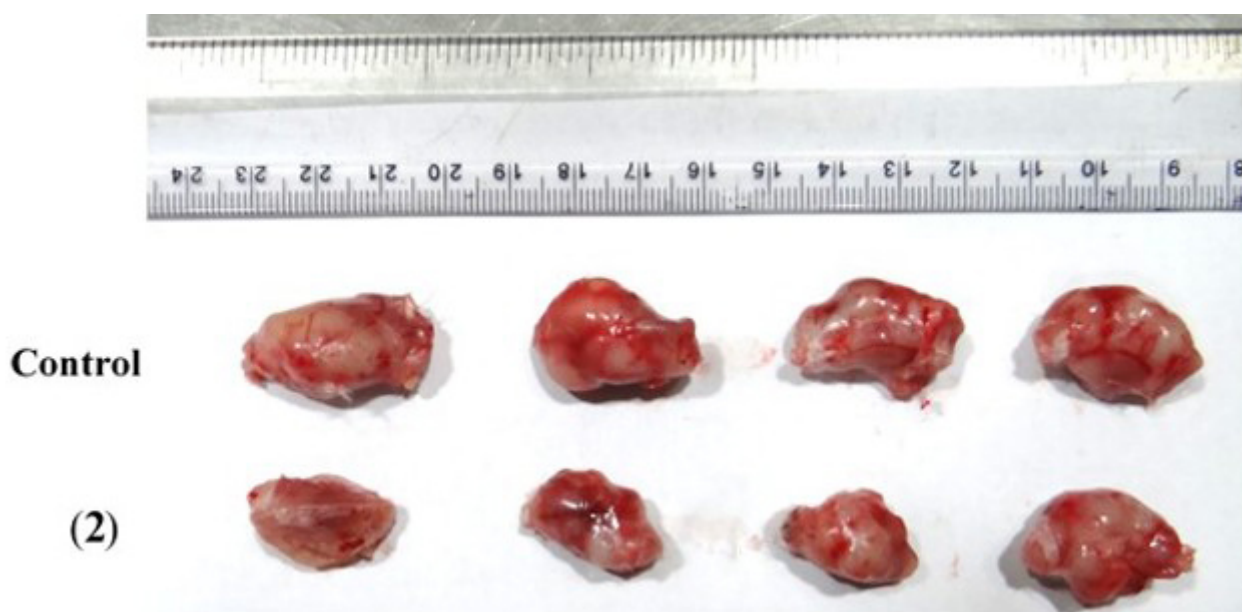


Figure 7. Comparison of 4T1 mammary tumors during in vivo treatment of tumors with $[\text{Ir}(\text{TPQ})_2(4\text{-EO}_2\text{-pic})]$ (**2**) complex.

The study of treatment of $[(\text{TPQ})_2\text{Ir}(4\text{-EO}_2\text{-pic})]$ (**2**) complex (10 mg/kg) was performed to evaluate the inhibition of the growth of the tumor as compared to a PBS buffer control until the size of the tumor in mice, which were administered with buffer control, grew to $\sim 1,500 \text{ mm}^3$. Later, the mice were sacrificed via saturated CO_2 euthanasia. Then, the tumors were extracted via surgery. The tumor images in response to treatments with $[(\text{TPQ})_2\text{Ir}(4\text{-EO}_2\text{-pic})]$ (**2**) complex (10 mg/kg) in comparison with a control of PBS buffer are shown in Figure 7.

Discussion

The ^1H NMR (in CDCl_3) for the complexes (**1–3**) has exhibited the chemical shifts depending on electron densities around the protons. The $^{13}\text{C}\{^1\text{H}\}$ resonances were exhibited for aryl as well as for aliphatic protons in the case of $[(\text{TPQ})_2\text{Ir}(4\text{-EO}_2\text{-pic})]$ (**2**) and $[(\text{ppy})_2\text{Ir}(\text{dfpmpy})]$ (**3**) complexes.

The two absorbance bands observed at wavelengths (λ) 312 nm and 421 nm are attributable to $\pi\text{-}\pi^*$ transitions of the ligands, and a shoulder at 459 nm is attributable to MLCT (metal-to-ligand charge transfer) transitions. A weaker band seen at λ 578 nm is attributable to a spin-forbidden MLCT transition. The PL spectrum of $[(\text{TPQ})_3\text{Ir}]$ (**1**) complex is presented in. The PL spectrum of $[(\text{TPQ})_3\text{Ir}]$ (**1**) complex exhibits a red emission peak at 601 nm upon excitation with λ 430 nm, owing to the donor-acceptor system in the cyclometallated ligand. The UV-Vis absorption and emission (PL) spectra of $[\text{Ir}(\text{TPQ})_2(4\text{-EO}_2\text{-pic})]$ (**2**) complex were recorded at ambient temperature in acetonitrile. The strong absorptions in the UV region at λ ranging from 280 to 370 nm are attributable to spin-allowed $\pi\text{-}\pi^*$ transitions of the phenyl quinoline moiety of ligands. The weak bands in the visible range of wavelength λ 406–576 nm are attributable to the mixed singlet and triplet MLCT and intra-ligand CT transitions. The complex $[(\text{TPQ})_2\text{Ir}(4\text{-EO}_2\text{-pic})]$ (**2**) exhibited a single broad red emission centered at wavelength \sim 625 nm upon excitation by 583, 554, and 443 nm wavelengths (Figure 2).

The band at λ 354 nm is observed due to a singlet ($^1\text{MLCT}$) transition. The bluish-green emission was observed at a maximum of \sim 510 nm upon excitation by 465 nm in the emission spectra of $[(\text{ppy})_2\text{Ir}(\text{dfpmpy})]$ (**3**) complex [31].

The $[(\text{TPQ})_2\text{Ir}(4\text{-EO}_2\text{-pic})]$ (**2**) complex was found to be cytotoxic with substantially higher efficiency ($\text{IC}_{50} = 60 \mu\text{M}$) as compared to $[(\text{TPQ})_3\text{Ir}]$ (**1**) and $[(\text{ppy})_2\text{Ir}(\text{dfpmpy})]$ (**3**) complexes, which have been depicted in Figure 3. Among the three Ir(III) complexes, the $[(\text{TPQ})_2\text{Ir}(4\text{-EO}_2\text{-pic})]$ (**2**) complex has exhibited better anticancer activity. The structural features of $[(\text{TPQ})_2\text{Ir}(4\text{-EO}_2\text{-pic})]$ (**2**) complex with a polar organic side chain conferring a better amphiphilic nature lead to its better chances for internalization in cancer cells and eventually better anticancer potency.

The cellular internalization exhibited by the test $[\text{Ir}(\text{TPQ})_2(4\text{-EO}_2\text{-pic})]$ (**2**) complex in MDA-MB-231 and 4T1 mammary carcinoma cell lines, as observed on flow cytometry at 3 and 6 h after treatment. The enhanced cellular uptake $[\text{Ir}(\text{TPQ})_2(4\text{-EO}_2\text{-pic})]$ (**2**) complex with an increase in incubation time in both TNBC cells, i.e., MDA-MB-231 and 4T1 mammary carcinoma cells, is attributable to higher chances of interactions among the test $[\text{Ir}(\text{TPQ})_2(4\text{-EO}_2\text{-pic})]$ (**2**) and cellular membranes. Further, we state that during the cell culture experiments, it cannot be proven whether mycoplasma contamination occurred, and that there was no STR identification as well. We are unable to provide the relevant test results for the mycoplasma contamination.

The cellular internalization plays a crucial role in the potency of a complex to exhibit cytotoxicity. As per earlier reports and diverse mechanisms, we have discussed in the introduction, we can state that the antiproliferative or anticancer mechanism of the test drugs of test $[(\text{TPQ})_2\text{Ir}(4\text{-EO}_2\text{-pic})]$ (**2**) complex also proceeds through cellular internalization, accumulation in the nucleus, followed by DNA binding and its damage. Although the Ir(III) complexes have been shown to induce apoptosis via their interaction with mitochondria, leading to mitochondrial dysfunction [35] and lysosome targeting leading to lysosome disruption or loss of lysosomal integrity, which is able to cause cell death via a path called lysosomal membrane permeabilization (LMP) [36], releasing diverse enzymes like cathepsins, which are regulatory or important targets in cancer cell apoptosis [36, 37] as depicted in literature, the in-depth biochemical or biological mechanism may also be studied. However, our objective was to identify the appropriate, highly potent Ir(III) compounds. Since the test compounds have exhibited moderate antiproliferative activity, we have limited our mechanistic studies to the cellular internalization level. In our future efforts, the most potent Ir(III) compounds may be explored for their in-depth mechanistic studies at sub-cellular levels.

For this objective, the tumor induction in mice had to be performed. Although $[(\text{TPQ})_2\text{Ir}(4\text{-EO}_2\text{-pic})]$ (**2**) complex exhibited higher uptake in MDA-MB-231 cell lines, the model developed in nude mice by injecting

MDA-MB-231 cell lines was our choice of preference, which is possible in nude mice, which were not available. Hence, we planned to develop the tumor models in BALB/c mice. The development of MDA-MB-231 cell-induced tumors in BALB/c mice is not feasible. It may be possible only when BALB/c mice are immunosuppressed, which were not available. Hence, we have used the 4T1 cells induced tumor models for our studies. It should be noted that the 4T1 cells grow aggressively in BALB/c mice since they are a syngeneic model (same genetic background as BALB/c), allowing them to evade immune rejection and mimic human metastatic breast cancer. Hence, to study the anticancer/anti-proliferative properties, we have induced the 4T1 breast cancer cells to develop a tumor model in BALB/c mice, which is known to mimic human Stage IV breast cancer, which is aggressive, metastatic, and appropriate for studying TNBC [38–41].

The study of treatment of [(TPQ)₂Ir(4-EO₂-pic)] (2) complex (10 mg/kg) exhibited effective inhibition of the growth of the tumor as compared to a PBS buffer control when evaluated until the size of the tumor in mice, which were administered with buffer control, grew to ~1,500 mm³. Later, the mice were sacrificed via saturated CO₂ euthanasia. Then, the tumors were extracted via surgery. The tumor images in response to treatments with [(TPQ)₂Ir(4-EO₂-pic)] (2) complex (10 mg/kg) in comparison with a control of PBS buffer are shown in Figure 7.

The tumor size images on a scale bar in response to treatments with [(TPQ)₂Ir(4-EO₂-pic)] (2) complex (10 mg/kg) showed moderate inhibition of tumor growth in comparison with a control of PBS buffer. This study indicated a therapeutic effect of [Ir(TPQ)₂(4-EO₂-pic)] (2) complex formulation (10 mg/kg) in vivo. Although in our case we have not evaluated the cytotoxicity mechanism of Ir(III) complexes, earlier reports have explained the mechanism of similar Ir(III) complexes (Figure 8) with pyridyl, polypyridyl, or heterocyclic ligand-based moieties. Earlier in the introduction part, we mentioned the diverse mechanistic steps involved in the anticancer or cytotoxic effect of Ir(III) complexes.

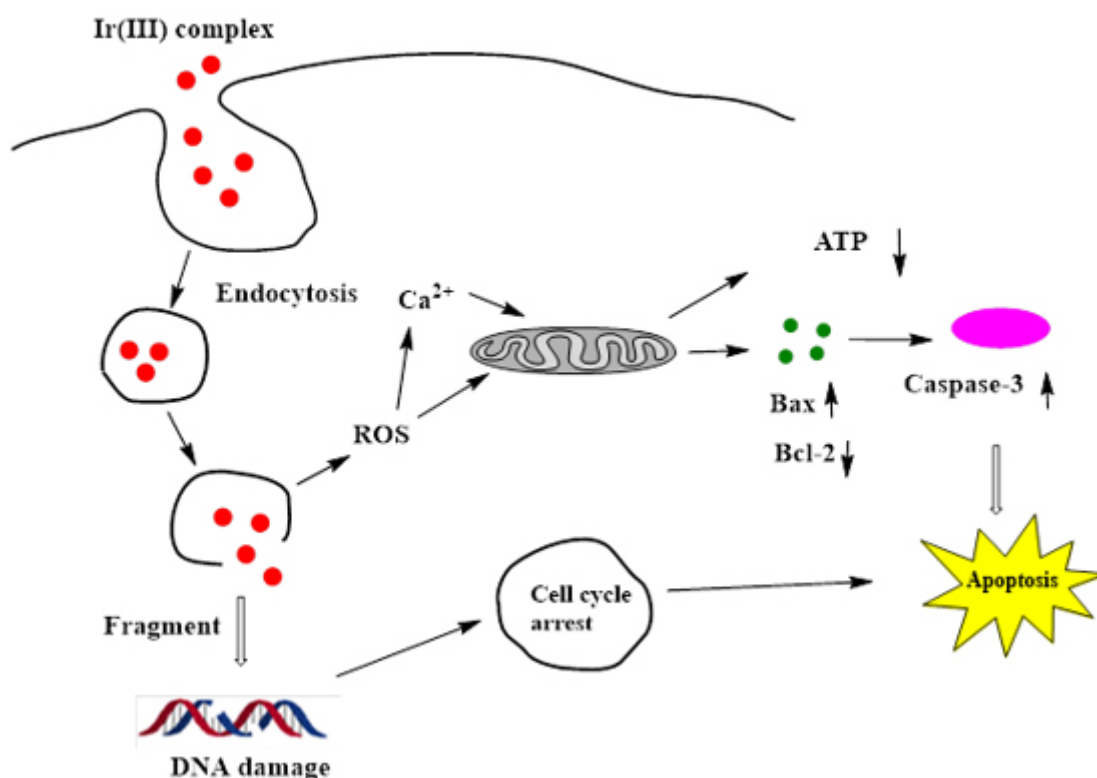


Figure 8. General mechanism of cancer cell killing by Ir(III) complexes. ROS: reactive oxygen species.

We anticipate that our test [(TPQ)₂Ir(4-EO₂-pic)] (2) complex may have a similar mechanism for tumor growth inhibitory activity [42–44]. Regarding this test complex, we would like to evaluate it further for the bio-imaging utility. The rationale behind exploring this application is the fact that it has a moderate

inhibitory property. Since $[(\text{TPQ})_2\text{Ir}(4\text{-EO}_2\text{-pic})]$ (**2**) complex has exhibited emission at ~ 625 nm, which is known to belong to the therapeutic or biological, or tissue transparency window. It is known that the biomolecules in cells do not emit in this region, and hence the auto-fluorescence caused by them is inhibited in the case of photo-luminescence employed in bio-medical applications. Hence, the emissions of test complexes are not affected by any other emissions (i.e., noise), and the evaluation results are contributed solely by test complexes. In this regard, red emission of $[(\text{TPQ})_3\text{Ir}]$ (**1**) complex but with poor cytotoxicity may be helpful for bio-imaging applications after appropriate functionalization with tumor targeting moieties like peptides or antibodies. While in the case of $[(\text{TPQ})_2\text{Ir}(4\text{-EO}_2\text{-pic})]$ (**2**) complex, its property of red emission as well as moderate cytotoxicity confers a potential of theragnostic utility to this test complex. Additionally, the $[(\text{TPQ})_2\text{Ir}(4\text{-EO}_2\text{-pic})]$ (**2**) complex has the potential to be evaluated for photodynamic therapy due to its moderate cytotoxicity and luminescence. Hence, we feel that the $[(\text{TPQ})_2\text{Ir}(4\text{-EO}_2\text{-pic})]$ (**2**) complex has the potential to be explored further for its theragnostic utility in biomedical applications in cancer management.

Furthermore, in the course of time, we have witnessed the development of artificial intelligence (AI) based techniques useful in drug discovery. In the management of breast cancer, AI is playing a crucial role. The employment of AI in anticancer drug development is improving the pharmaceutical domain, giving the design of novel potential drugs and the prediction of toxicity of drugs via computer-designed active biomolecular structures and tumor cell signaling networks, along with more personalized and effective treatments. AI fosters all phases of drug development, like preclinical, clinical trial design, recruitment of patients, and analysis of trials. The in-silico clinical trials lead to the prediction of patient responses and treatment outcomes, giving an excellent understanding which regularize and improves each phase. Among the diverse inputs from AI tools, the molecular modelling via docking and molecular dynamics studies has a great influence on the binding of drugs with target biomolecules (like proteins or DNA) to exhibit anticancer applications. The effective and desired binding is essential for the anticancer effect. This binding step regulates the anticancer or antiproliferative efficiency of the drug molecule. Additionally, it can predict whether any undesired interactions (which lead to side effects) are possible, indirectly stating the toxicity of the compounds. In this way, the AI-based tools can support the design of drugs, functional formulations, DDS, and treatment approaches to create conditions that do not cause serious harm from the perspective of breast cancer. In this regard, we would like to mention that Tabasi et al. [45] have performed excellent work where the docking and molecular dynamics studies were utilized to simulate the interaction of an anticancer, anti-inflammatory, antioxidant drug, i.e., curcumin, with α -lactalbumin and β -lactoglobulin and revealed the insights about their bindings, which revealed the strategies for potential therapeutic utility of curcumin in nano-formulations. Similarly, the directives from AI-based studies are anticipated to give more effective drugs to treat a deadly TNBC, along with fewer side effects or harm to the patient. In our future endeavours, our top priority will be the employment of AI-based techniques for the development of Ir(III) based complexes with enhanced potential as differential anticancer drugs, along with the ability for bio-imaging, i.e., theragnostic utility. But at this point, we analyzed that the work related to these test complexes has given us direction for search or rational design of new Ir(III) complexes for theragnostic and multimodal applications in cancer management with the help of AI-based techniques. In conclusion, we have synthesized Ir(III) complexes possessing biocompatibility and pharmacologically active pyridyl-based ligands. The complexes exhibited cytotoxicity against rapidly invading TNBC cell lines (MDA-MB-231 and 4T1) in vitro as well as in vivo tumor inhibitory property against 4T1 mammary carcinoma induced in the BALB/c model. Additionally, they exhibited green to red emissions, which proved appropriate for bio-imaging applications since they were observed to internalize in TNBC cancer cells within 3 h, which enhanced at 6 h as evidenced by flow cytometry and confocal microscopy. These studies revealed the appropriate internalization and theragnostic utility of the test Ir(III) complexes like $[(\text{TPQ})_2\text{Ir}(4\text{-EO}_2\text{-pic})]$ (**2**) complex confer them potency for their further studies in cancer treatment as theragnostic agents.

Abbreviations

3D: three-dimensional

AI: artificial intelligence

C₆H₁₄: hexane

CDCl₃: deuterated chloroform

CH₂Cl₂: dichloromethane

CH₃COOCH₂CH₃: ethyl acetate

CPCSEA: Committee for the Purpose of Control and Supervision of Experiments on Animals

DAPI: 4',6-diamidino-2-phenylindole

DDS: drug delivery systems

DMEM: Dulbecco's modified Eagle medium

DMSO: dimethyl sulfoxide

ER: estrogen receptor

FBS: fetal bovine serum

FDA: Food and Drug Administration

HMGR: HMG-CoA reductase

HRMS: high-resolution mass spectrometry

Ir(III): iridium(III)

KMP: kaempferol

MLCT: metal-to-ligand charge transfer

MTT: 3-[4,5-dimethylthiazol-2-yl]-2,5 diphenyl tetrazolium bromide

N₂: nitrogen

NA: numerical aperture

NMR: nuclear magnetic resonance

PBS: phosphate-buffered saline

PL: photoluminescence

ppm: parts per million

Pt(II): platinum(II)

ROS: reactive oxygen species

RT: room temperature

TNBC: triple-negative breast cancer

TPQ: 4-phenyl-2-(thiophen-2-yl) quinoline

UV-Vis: ultraviolet-visible

Supplementary materials

The supplementary figures for this article are available at: https://www.explorationpub.com/uploads/Article/file/1008158_sup_1.pdf.

Declarations

Acknowledgments

The authors are thankful to Dr. Avdhesh Kumar, Associate Director, Chemistry Group, BARC, Dr. Niharendu Choudhuri, Head, Chemistry Division, BARC, Mumbai, and Dr. Tapas Das, Head, Radiopharmaceuticals Division (RPhD), BARC, Mumbai, for the encouragement and support. We are thankful to Mr. P. B. Dhakate from the Animal House Facility, BARC, for providing the BALB/c mice. One of the authors, LZ, is grateful to the Ministry of Tribal Affairs (MOTA), Government of India, New Delhi, for the award of National Fellowship for ST Students (NFST) to him for his higher education for pursuing a Ph.D. in Chemistry, as well as thankful to HRDD, BARC, for allowing him practical training at Chemistry Division, BARC.

Author contributions

PPP and SKS: Conceptualization, Investigation, Methodology. NSK, SKS, PPP, LZ, and CK: Investigation, Methodology. PPP and VS: Investigation, Methodology. PPP and SKS: Formal analysis, Writing—review & editing, Visualization. PPP, NSK, and SKS: Writing—original draft. All authors read and approved the submitted version.

Conflicts of interest

All the authors declare that they have no conflicts of interest.

Ethical approval

The study for tumor inhibitory studies in 4T1 mammary carcinoma mice model animal research was approved by the Institutional Animal Ethics Committee (BAEC No. 19/22) of BARC, Mumbai. All the animals used in this study were treated in accordance with the 'Guidelines for the Care and Use of Laboratory Animals'.

Consent to participate

Not applicable.

Consent to publication

Not applicable.

Availability of data and materials

The data can be obtained from the corresponding authors or from the supplementary materials.

Funding

This study was supported by internal funding from our institute, Bhabha Atomic Research Centre, Trombay, Mumbai-400085, India, belonging to the Department of Atomic Energy (DAE), Government of India. The funder had no role in study design, data collection and analysis, decision to publish, or preparation of the manuscript.

Copyright

© The Author(s) 2026.

Publisher's note

Open Exploration maintains a neutral stance on jurisdictional claims in published institutional affiliations and maps. All opinions expressed in this article are the personal views of the author(s) and do not represent the stance of the editorial team or the publisher.

References

1. Adhikari S, Nath P, Das A, Datta A, Baildya N, Duttaroy AK, et al. A review on metal complexes and its anti-cancer activities: Recent updates from *in vivo* studies. *Biomed Pharmacother.* 2024;171:116211. [DOI] [PubMed]
2. Liu L, Wang W, Huang S, Hong Y, Li G, Lin S, et al. Inhibition of the Ras/Raf interaction and repression of renal cancer xenografts *in vivo* by an enantiomeric iridium(III) metal-based compound. *Chem Sci.* 2017;8:4756–63. [DOI] [PubMed] [PMC]
3. Cao R, Jia J, Ma X, Zhou M, Fei H. Membrane localized iridium(III) complex induces endoplasmic reticulum stress and mitochondria-mediated apoptosis in human cancer cells. *J Med Chem.* 2013;56:3636–44. [DOI] [PubMed]
4. Cao J, Tan C, Chen M, Wu N, Yao D, Liu X, et al. Targeting cancer cell metabolism with mitochondria-immobilized phosphorescent cyclometalated iridium(III) complexes. *Chem Sci.* 2017;8:631–40. [DOI] [PubMed] [PMC]
5. Li C, Yu M, Sun Y, Wu Y, Huang C, Li F. A nonemissive iridium(III) complex that specifically lights-up the nuclei of living cells. *J Am Chem Soc.* 2011;133:11231–9. [DOI] [PubMed]
6. Ma X, Jia J, Cao R, Wang X, Fei H. Histidine-iridium(III) coordination-based peptide luminogenic cyclization and cyclo-RGD peptides for cancer-cell targeting. *J Am Chem Soc.* 2014;136:17734–7. [DOI] [PubMed]
7. Chen B, Pan N, Liao J, Huang M, Jiang D, Wang J, et al. Cyclometalated iridium(III) complexes as mitochondria-targeted anticancer and antibacterial agents to induce both autophagy and apoptosis. *J Inorg Biochem.* 2021;219:111450. [DOI] [PubMed]
8. Aderinto SO, John T, Onawole A, Galleh RP, Thomas JA. Iridium(III)-based minor groove binding complexes as DNA photocleavage agents. *Dalton Trans.* 2024;53:7282–91. [DOI] [PubMed]
9. Yang T, Zhu M, Jiang M, Yang F, Zhang Z. Current status of iridium-based complexes against lung cancer. *Front Pharmacol.* 2022;13:1025544. [DOI] [PubMed] [PMC]
10. Hao J, Liu H, Wang J, Wang X, Huang C, Liang L, et al. Iridium (III) complexes induce cervical carcinoma apoptosis via disturbing cellular redox homeostasis disorder and inhibiting PI3K/AKT/mTOR pathway. *J Inorg Biochem.* 2022;235:111946. [DOI] [PubMed]
11. Chen C, Guo Z, Ma G, Ma J, Zhang Z, Yu Q, et al. Lysosomal Fe²⁺ contributes to myofibrillar protein degradation through mitochondrial-dysfunction-induced apoptosis. *LWT.* 2021;143:111197. [DOI]
12. Xie K, Lu X, Zhu H, Zhu L, Li R, Ye R. Iridium(III) complexes conjugated with naproxen exhibit potent anti-tumor activities by inducing mitochondrial damage, modulating inflammation, and enhancing immunity. *Dalton Trans.* 2024;53:8772–80. [DOI] [PubMed]
13. Balachandran C, Yokoi K, Naito K, Haribabu J, Tamura Y, Umezawa M, et al. Cyclometalated Iridium(III) Complex-Cationic Peptide Hybrids Trigger Paraptosis in Cancer Cells via an Intracellular Ca²⁺ Overload from the Endoplasmic Reticulum and a Decrease in Mitochondrial Membrane Potential. *Molecules.* 2021;26:7028. [DOI] [PubMed] [PMC]
14. Zhang X, Yu L, Xu H. Lysosome calcium in ROS regulation of autophagy. *Autophagy.* 2016;12:1954–5. [DOI] [PubMed] [PMC]
15. Pradhan KC, Jadab M, Rout S, Dandela R, Mandal D, Parija T, et al. Orange/red light emitting iridium(III) organometallic complexes containing 2,3-di(pyridine-2-yl)quinoxaline as ancillary ligand and their anticancer properties. *Z anorg allg Chem.* 2023;649:e202300169. [DOI]
16. Sun L, Li G, Chen X, Chen Y, Jin C, Ji L, et al. Azo-Based Iridium(III) Complexes as Multicolor Phosphorescent Probes to Detect Hypoxia in 3D Multicellular Tumor Spheroids. *Sci Rep.* 2015;5:14837. [DOI] [PubMed] [PMC]
17. Ponram M, Balijapalli U, Sambath B, Kulathu Iyer S, Kakaraparthi K, Thota G, et al. Inkjet-printed phosphorescent Iridium(III) complex based paper sensor for highly selective detection of Hg²⁺. *Dyes Pigments.* 2019;163:176–82. [DOI]

18. Xin H, Huang Y, Han Y, Tang L, Yang G, Zhang Y, et al. A two-photon iridium(III) complex probe for sensitive detection of SO₂ derivatives in living cell mitochondria. *Spectrochim Acta A Mol Biomol Spectrosc.* 2023;299:122876. [DOI] [PubMed]
19. Sarlak S, Pagès G, Luciano F. Enhancing radiotherapy techniques for Triple-Negative breast cancer treatment. *Cancer Treat Rev.* 2025;136:102939. [DOI] [PubMed]
20. Riaz F, Gruber JJ, Telli ML. New Treatment Approaches for Triple-Negative Breast Cancer. *Am Soc Clin Oncol Educ Book.* 2025;45:e481154. [DOI] [PubMed]
21. Mulligan MP, Boudreau MW, Bouwens BA, Lee Y, Carrell HW, Zhu J, et al. Single Dose of a Small Molecule Leads to Complete Regressions of Large Breast Tumors in Mice. *ACS Cent Sci.* 2025;11:228–38. [DOI] [PubMed] [PMC]
22. Yuan H, Zhou L, Hu W, Yang M. LINC00626 drives tamoxifen resistance in breast cancer cells by interaction with UPF1. *Sci Rep.* 2025;15:2997. [DOI] [PubMed] [PMC]
23. Manna S, Holz MK. Tamoxifen Action in ER-Negative Breast Cancer. *Sign Transduct Insights.* 2016;5:1–7. [DOI] [PubMed] [PMC]
24. Scarpetti L, Oturkar CC, Juric D, Shellock M, Malvarosa G, Post K, et al. Therapeutic Role of Tamoxifen for Triple-Negative Breast Cancer: Leveraging the Interaction Between ER β and Mutant p53. *Oncologist.* 2023;28:358–63. [DOI] [PubMed] [PMC]
25. McCormick B, Wesson MF, Cox L, Osborne MP, Petrek JA, Kinne DW. Iridium-192 implants for primary breast cancer: experience with placement at the time of wide local excision. *Int J Radiat Oncol Biol Phys.* 1988;15:745–8. [DOI] [PubMed]
26. Ivanov O, Dickler A, Lum BYF, Pellicane JV, Francescatti DS. Twelve-month follow-up results of a trial utilizing Axxent electronic brachytherapy to deliver intraoperative radiation therapy for early-stage breast cancer. *Ann Surg Oncol.* 2011;18:453–8. [DOI] [PubMed]
27. Kalhori F, Yazdiani H, Khademozraeian F, Hamzkanloo N, Mokaberi P, Hosseini S, et al. Enzyme activity inhibition properties of new cellulose nanocrystals from *Citrus medica* L. pericarp: A perspective of cholesterol lowering. *Luminescence.* 2022;37:1836–45. [DOI] [PubMed]
28. Markowska A, Antoszczak M, Markowska J, Huczyński A. Statins: HMG-CoA Reductase Inhibitors as Potential Anticancer Agents against Malignant Neoplasms in Women. *Pharmaceuticals (Basel).* 2020;13:422. [DOI] [PubMed] [PMC]
29. Kaffash M, Tolou-Shikhzadeh-Yazdi S, Soleimani S, Hoseinpoor S, Saberi MR, Chamani J. Spectroscopy and molecular simulation on the interaction of Nano-Kaempferol prepared by oil-in-water with two carrier proteins: An investigation of protein-protein interaction. *Spectrochim Acta A Mol Biomol Spectrosc.* 2024;309:123815. [DOI] [PubMed]
30. Giridhar T, Han T, Cho W, Saravanan C, Lee T, Jin S. An easy route to red emitting homoleptic IrIII complex for highly efficient solution-processed phosphorescent organic light-emitting diodes. *Chem Eur J.* 2014;20:8260–4. [DOI] [PubMed]
31. Giridhar T, Lee J, Cho W, Yoo H, Moon C, Kim J, et al. Highly efficient bluish green phosphorescent organic light-emitting diodes based on heteroleptic iridium(III) complexes with phenylpyridine main skeleton. *Org Electron.* 2014;15:1687–94. [DOI]
32. Zhang KY, Zhang T, Wei H, Wu Q, Liu S, Zhao Q, et al. Phosphorescent iridium(III) complexes capable of imaging and distinguishing between exogenous and endogenous analytes in living cells. *Chem Sci.* 2018;9:7236–40. [DOI] [PubMed] [PMC]
33. Zhu J, Yiu S, Tang BZ, Lo KK. Luminescent Neutral Cyclometalated Iridium(III) Complexes Featuring a Cubic Polyhedral Oligomeric Silsesquioxane for Lipid Droplet Imaging and Photocytotoxic Applications. *Inorg Chem.* 2021;60:11672–83. [DOI] [PubMed]
34. Kamiloglu S, Sari G, Ozdal T, Capanoglu E. Guidelines for cell viability assays. *Food Front.* 2020;1:332–49. [DOI]

35. Lin H, Wei J, Yao W, Zhang Q, Jin J. A cyclometalated iridium(III) complex induces paraptotic cell death via mitochondrial dysfunction and ER stress in triple-negative breast cancer cells. *Front Pharmacol.* 2026;17:1739226. [DOI] [PubMed] [PMC]
36. He L, Li Y, Tan CP, Ye RR, Chen MH, Cao JJ, et al. Cyclometalated iridium(III) complexes as lysosome-targeted photodynamic anticancer and real-time tracking agents. *Chem Sci.* 2015;6:5409–18. [DOI] [PubMed] [PMC]
37. Liu J, Yang L, Tian H, Ma Q. Cathepsin D is involved in the oxygen and glucose deprivation/reperfusion-induced apoptosis of astrocytes. *Int J Mol Med.* 2016;38:1257–63. [DOI] [PubMed]
38. Pulaski BA, Ostrand-Rosenberg S. Mouse 4T1 breast tumor model. *Curr Protoc Immunol.* 2001; Chapter 20:Unit 20.2. [DOI] [PubMed]
39. Schrörs B, Boegel S, Albrecht C, Bukur T, Bukur V, Holtsträter C, et al. Multi-Omics Characterization of the 4T1 Murine Mammary Gland Tumor Model. *Front Oncol.* 2020;10:1195. [DOI] [PubMed] [PMC]
40. Tao K, Fang M, Alroy J, Sahagian GG. Imagable 4T1 model for the study of late stage breast cancer. *BMC Cancer.* 2008;8:228. [DOI] [PubMed] [PMC]
41. Martín-Pardillos A, Valls Chiva Á, Bande Vargas G, Hurtado Blanco P, Piñeiro Cid R, Guijarro PJ, et al. The role of clonal communication and heterogeneity in breast cancer. *BMC Cancer.* 2019;19:666. [DOI] [PubMed] [PMC]
42. Zhang L, Gu Y, Wang Y, Bai L, Du F, Zhang W, et al. Design, Synthesis, and Anticancer Effect Studies of Iridium(III) Polypyridyl Complexes against SGC-7901 Cells. *Molecules.* 2019;24:3129. [DOI] [PubMed] [PMC]
43. Xie F, Wang Y, Zhu J, Xu H, Guo Q, Wu Y, et al. Anticancer mechanism studies of iridium(III) complexes inhibiting osteosarcoma HOS cells proliferation. *J Inorg Biochem.* 2022;237:112011. [DOI] [PubMed]
44. Yi Q, Zhang W, He M, Du F, Wang X, Wang Y, et al. Anticancer and antibacterial activity in vitro evaluation of iridium(III) polypyridyl complexes. *J Biol Inorg Chem.* 2019;24:151–69. [DOI] [PubMed]
45. Tabasi M, Maghami P, Amiri-Tehranizadeh Z, Reza Saberi M, Chamani J. New perspective of the ternary complex of nano-curcumin with β -lactoglobulin in the presence of α -lactalbumin: Spectroscopic and molecular dynamic investigations. *J Mol Liq.* 2023;392:123472. [DOI]